Creep Tests on Rock Salt with Changing Load as a Basis for the Verification of Theoretical Material Laws

K. H. Lux and S. Heusermann

University of Hannover,
Hannover, Federal Republic of Germany

ABSTRACT

To describe the viscose material behavior of rock salt international literature recommends constitutive laws which markedly differ not only in the parameters quoted but also in the basic theoretical statement. The alternative use of several constitutive laws in project design can lead to vast differences in the predicted long-term behavior of a storage cavern in the rock salt mass and so to the question as to which constitutive law formulation can produce a realistic estimation of viscose displacements even with extrapolations over longer periods.

To clarify this question, step loading tests have been carried out at the Institute for Underground Construction additional to the usual creep tests at constant stress. These step loading tests were run both with increasing as well as decreasing deviatoric stress. This paper shows that the creep behavior measured under constant stress can be described by almost all constitutive laws with appropriate parameter selection. With extrapolations beyond the laboratory test time, large differences in the predicted viscose displacements occur, even with these simple boundary conditions. However, already within the laboratory period large differences occur if step loading tests with load increase or load decrease are recalculated using various constitutive laws. Only few laws prove suitable.

Additional to these comparison tests the results of creep tests under triaxial extension stress conditions using axially perforated samples are first compared to those obtained from theoretical constitutive laws. Due to the change in the geometric conditions of the sample more possibilities of constitutive law identification for rock salt on the basis of laboratory tests are produced.

INTRODUCTION AND AIMS

Over the last few years, the construction of underground cavities in rock salt has become increasingly significant, in particular because of public discussions on the possibility of using salt domes for the final disposal of radioactive waste. This interest has been reflected in the appearance of numerous research projects and publications. In addition to this particular use of salt mines in the future, the construction of underground cavities in salt deposits is currently important for the recovery of rock salt and potash in conventional mines. The construction of salt caverns by solution mining is also significant, on the one hand as an alternative technique for the recovery of rock salt, and on the other hand to provide underground cavities for the storage of liquid or gaseous products, e.g., natural gas. Independent of the specific application of the cavity, a fundamental requirement is placed on the operator to design the cavern in such a way that public safety is not endangered, and to ensure optimum utilization of the deposit from the point of view of economics. Furthermore, it is also desirable to be able to develop an optimum design from the viewpoint of operating costs, while considering boundary conditions specific to the project.

A prerequirement for a rock-mechanical design process which satisfies these objectives is the development of theoretical models relating to the characteristics of cavity construction and operation in rock salt. These models can form the basis of both realistic and well-founded predictions of the mechanical behavior of the rock mass, following comparison and verification with field observations. A major area of research currently taking place at the Institut für Unterirdisches Bauen (LUB) of the University of Hanover is focused on the development of such models (Lux, 1983 and Heusermann, Lux and Rokahr, 1982).

In addition to the determination of rock mass stresses, a rock-mechanical design also requires estimation of the rock deformation to be expected—particularly from the point of view of possible local or progressive creep failure of the rock and/or the long-term usability of the cavity. A prerequirement of such a prediction is the formulation of a material law that is able to describe the viscous behavior of the in situ rock salt under consideration of the in situ stress and temperature. Based on laboratory tests, a num-

ber of widely differing formulations have been proposed in the literature. However, their application in project planning leads to considerable differences in the predictions obtained, according to which formulation is used, and thus leads to considerable doubts on the degree of confidence which one can attach to the use of theoretical models for such purposes. This, then, led to the question of whether laboratory tests—which have the advantage over field tests of guaranteeing clear geometric and stress test conditions—are able to indicate a preference for any particular formulation.

The following paper describes a comparative investigation in which five qualitatively different formulations of the material laws were considered. Because the material parameters quoted in the literature were determined for different types of rock salt, and furthermore, since their determination is influenced by the respective test conditions in each of the investigations, their comparison appears meaningless. For this reason, based on a set of creep curves, the parameters were determined once again for all five formulations under consideration, followed by a comparison of the measured and the calculated creep strain and creep rate for each of the formulations, not only considering creep tests with constant load over the usual timescales of laboratory tests, but also extrapolated to longer times, and considering additional creep tests with step-wise stress increase and stress decrease. Furthermore, the results of creep tests on samples with axial holes are discussed, together with comments on their significance for the verification of the suitability of particular formulations of the material laws.

ALTERNATIVE FORMULATIONS OF THE MATERIAL LAWS

The following material laws were considered in the following comparative investigation:

1. Material law according to Boresi/Deere (1963), (time hardening):

$$\dot{\epsilon}(t) = m \cdot a \cdot \sigma_v^n \cdot t^{m-1} \tag{1}$$

2. Material law according to Menzel/Schreiner (1977), (strain hardening):

$$\dot{\epsilon}(\epsilon^v) = a^* \cdot \sigma_v^{n^*} \cdot (\epsilon_v^v)^{-\alpha} \tag{2}$$

3. Material law according to Odqvist/Hult (1962), (total strain theory):

$$\epsilon^v(t) = a \cdot \sigma_v^n \tag{3a}$$

$$\epsilon^v(t) = \epsilon_{tr}^v(\sigma_v) + a \cdot \sigma_v^n \cdot t \tag{3b}$$

4. Material law according to McVetty/Hunsche (Hunsche, 1981), (additive superposition of the transient creep rate with time hardening and a constant secondary creep rate):

$$\dot{\epsilon}(t) = b \cdot m \cdot e^{-m \cdot t} \cdot \exp(-Q_1/RT) \cdot \sigma_v^{n_1} + a \cdot \exp(-Q_2/RT) \cdot \sigma_v^{n_2} \tag{4a}$$

$$\epsilon^v(t) = b \cdot \exp(-Q_1/RT) \cdot \sigma_v^{n_1} \cdot (1 - e^{-m \cdot t}) + a \cdot \exp(-Q_2/RT) \cdot \sigma_v^{n_2} \cdot t \tag{4b}$$

5. Material law LUBBY 2, (Heusermann, Lux, and Rokahr, 1982), (additive superposition of the transient creep rate with time or strain hardening and a constant secondary creep rate):

$$\dot{\epsilon}(t) = \left[\frac{1}{3\,\eta_K(\sigma_v)} \exp\left(-\frac{G_K(\sigma_v)}{\eta_k(\sigma_v)} \cdot t \right) + \frac{1}{3\,\eta_m(\sigma_v)} \right] \cdot \sigma_v \tag{5a}$$

or

$$\dot{\epsilon}(\epsilon_{tr}^v) = \left[\frac{1}{3\,\eta_K(\sigma_v)} \cdot \left(1 - \frac{\epsilon_{tr}^v}{\sigma_v} \cdot 3\,G_K(\sigma_v) \right) + \frac{1}{3\,\eta_M(\sigma_v)} \right] \cdot \sigma_v \tag{5b}$$

The influence of temperature can be taken account of in Formulation 5 either by carrying out the tests at the corresponding in situ rock temperature or by investigating not only the stress dependency but also the temperature dependency of the material parameters G_k, η_k and η_m.

It is important to be aware of the fact that the parameters used in the above five formulations are not necessarily identical even if the same abbreviations are used. This is particularly true of the pre-factors. For abbreviation it is defined:

$$3\eta_M = \bar{\eta}_M, 3G_K = \bar{G}_K, 3\eta_K = \bar{\eta}_K \tag{5c}$$

LABORATORY FACILITIES AVAILABLE AT LUB

The laboratory equipment available at LUB, which is installed in two controlled-environment rooms, can be seen in Figures 1 and 2.

A servo-hydraulically controlled triaxial press, which is designed for a vertical load of up to 2500 kN is illustrated in Figure 1. The high pressure cell allows a pressure of up to 50 MPa to be applied to the sample. The apparatus accommodates samples with dimensions of up to h = 250 mm and d = 100 mm, but generally the dimensions of the samples investigated were h/d = 180/90 mm. The vertical pressure can either be regulated in proportion to the load, strain or deformation of the samples. In addition to uniaxial compression tests (UC), triaxial compression tests (TC) and triaxial extension tests (TE) can also be carried out.

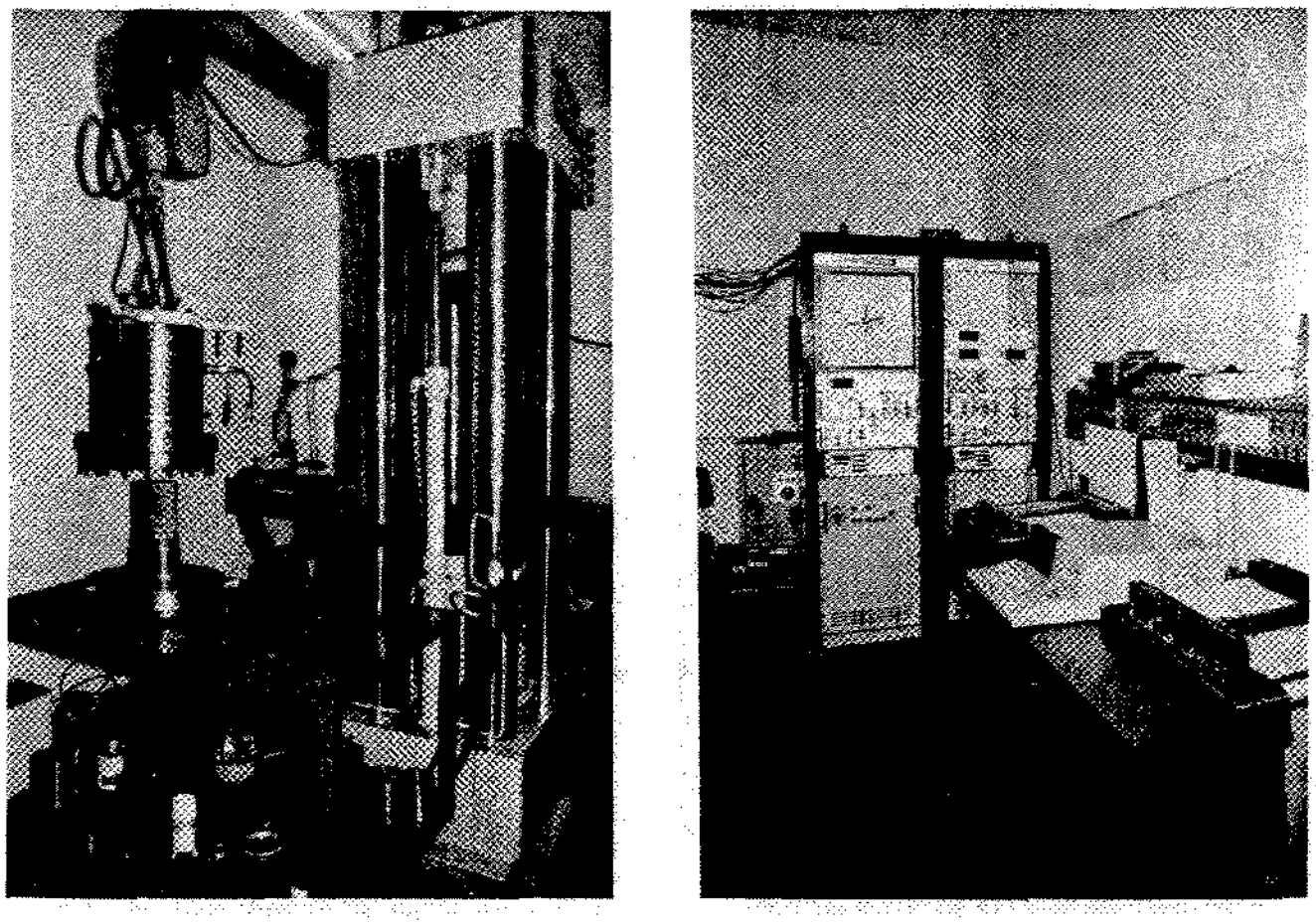

Figure 1. Triaxial press in Laboratory 1 of the Institute for Underground Construction.

The deformation was measured with inductive transducers (LVDT). The results were then plotted as load-displacement or displacement-time diagrams. The measured values were simultaneously digitalized and fed into a microcomputer for further processing.

The available creep rigs, which are also servo-hydraulically controlled are shown in Figure 2. Two creep rigs are available for tests at room temperature, each of which can accommodate up to five samples simultaneously, in order to be able to generate sufficient data for evaluation in a relatively short period of time. Generally, three samples were investigated simultaneously.

During creep tests, the load is regulated in accordance with the deformation, in order to guarantee a constant stress over the duration of the test. Two special creep rigs are also available for use at temperatures of up to $+250°C$ and down to $-80°C$. In the temperature range of approximately $+50°C$ to $-80°C$, the deformation can be recorded as before with inductive transducers. At higher temperatures, it is necessary to measure the deformation by using a special optical system. Data acquisition took place via a multi-channel recorder, which generated a printout and simultaneously fed the digitalized parameters to a microcomputer for further evaluation.

CREEP TESTS AND PROCESSING OF THE MEASURED DATA

Data from two uniaxial multiple-stage creep tests of rock salt from the Asse mine were used for the purposes of the comparative investigation under consideration. The salt samples were fine to medium crystalline rock salt of the Staßfurt series (Na 2), and were without impurities and without marked crystalline orientation. The uniaxial compressive strength of this material was $\sigma_u \cong -27$ MPa.

Figures 3 and 4 show the creep strain ϵ^v and the creep rate $\dot{\epsilon}^v$ for both samples in relationship to time, as obtained via creep tests with step-wise stress increase. The creep strain is plotted with a linear scale and the creep rate is plotted with a semi-logarithmic scale. Stress steps of $\sigma = 12$, 14 and 16 MPa were used for test no. 5/1 and stress steps of $\sigma = 16$, 18 and 20 MPa for test no. 2/2. (Note that in the following analysis, for reasons of simplicity, values for stress and for the resulting strain are both considered to be positive in sign). The time duration of the steps was not

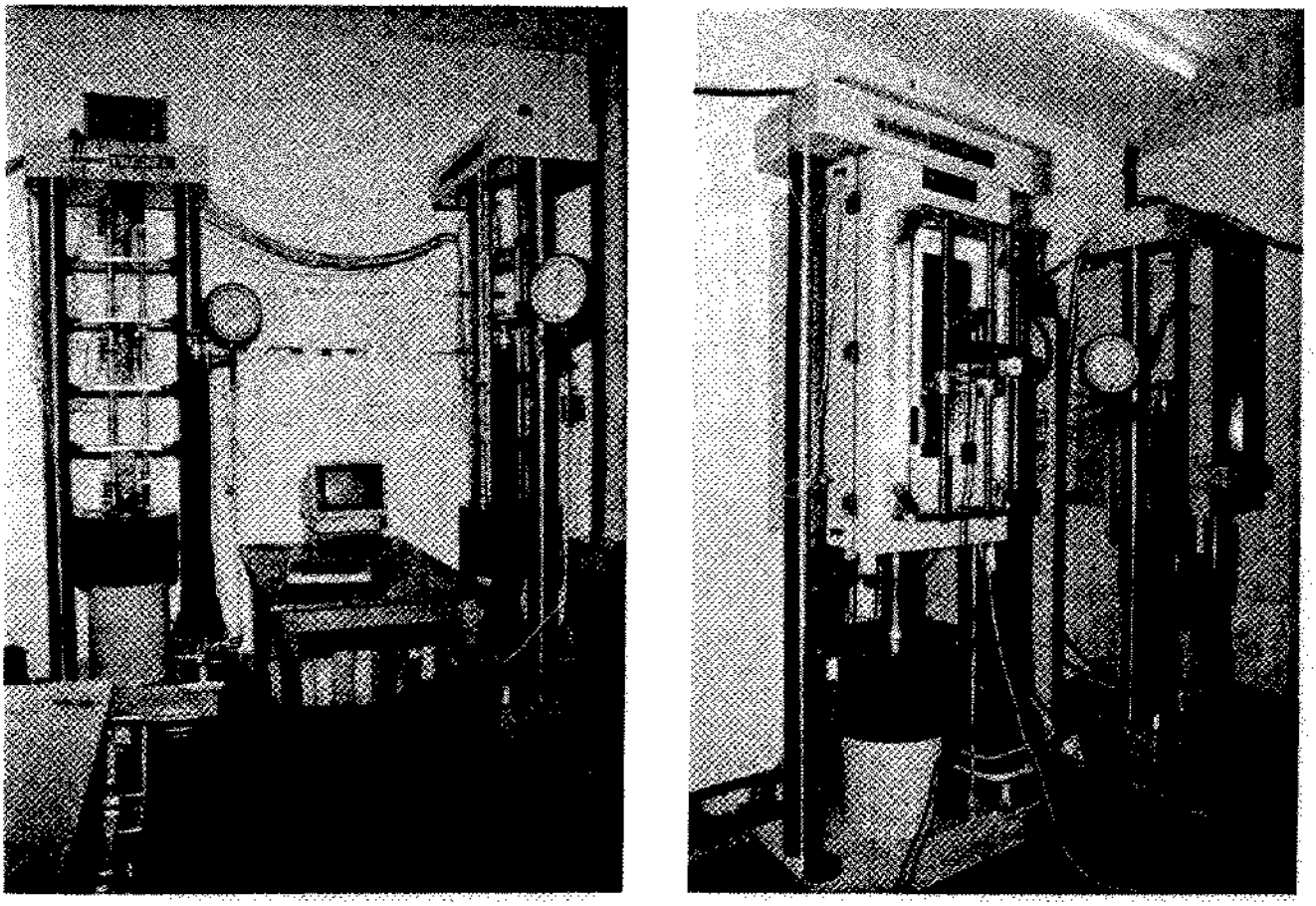

Figure 2. Creep rigs in Laboratory 2 of the Institute for Underground Construction.

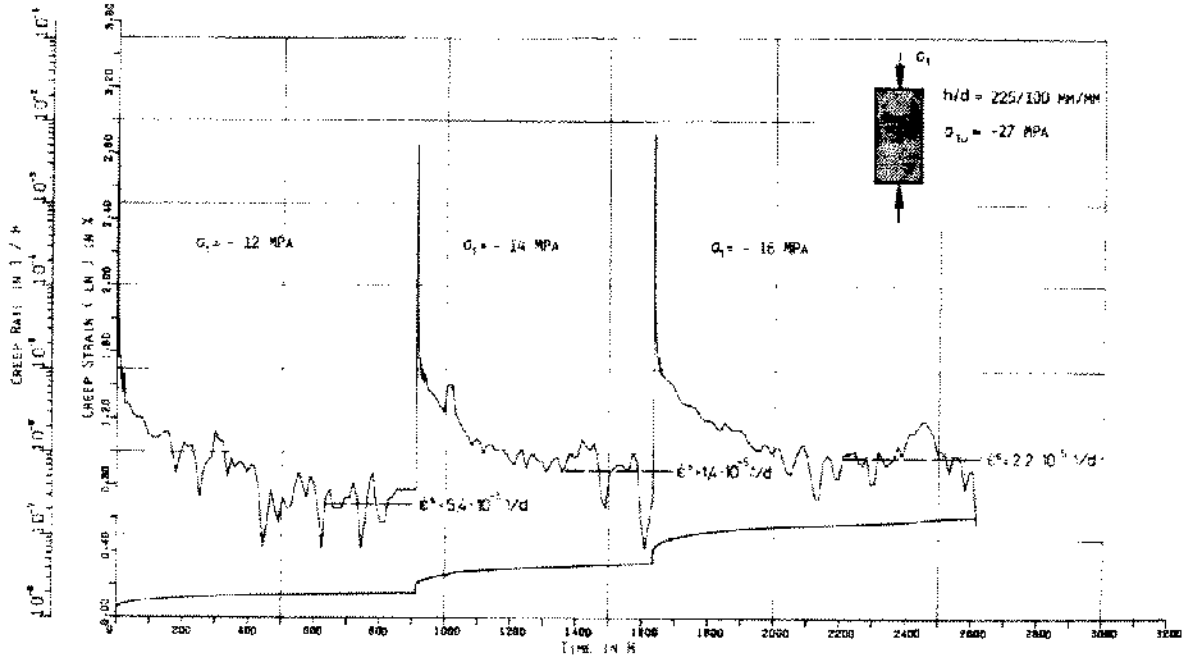

Figure 3. Multi-stage creep test AS-5/1.

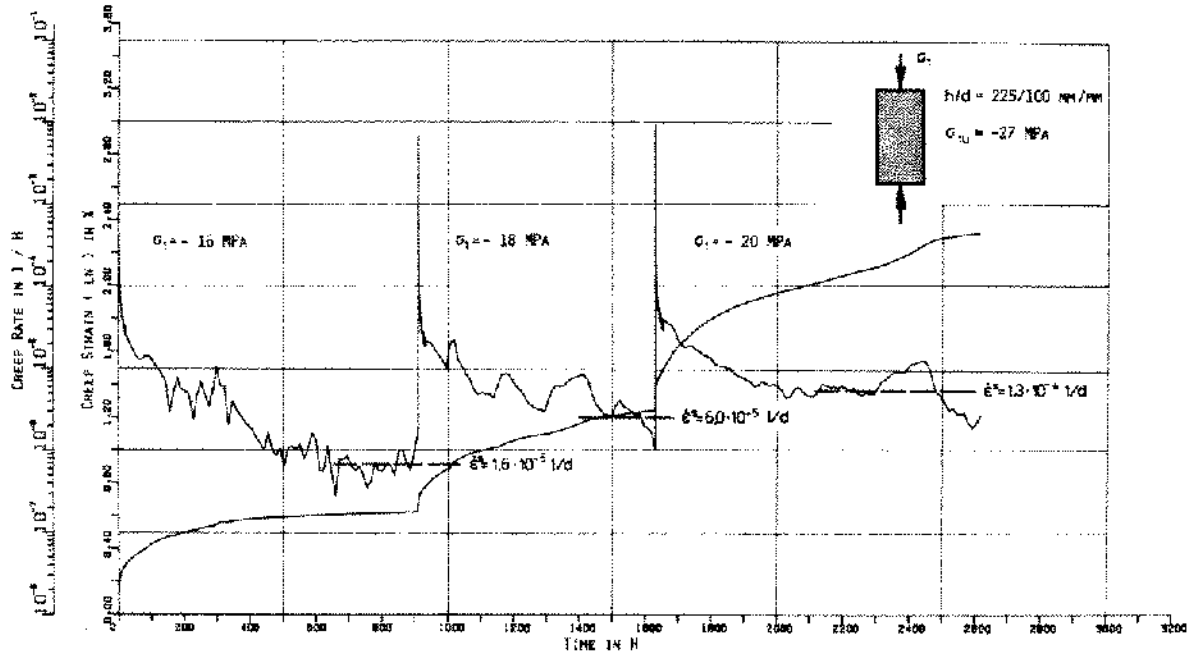

Figure 4. Multi-stage creep test AS-2/2.

constant—it lay between 700 and 1,000 h. The test temperature was 295 °K and the air humidity approximately 40%. The vertical load was regulated to maintain a constant stress σ in accordance with the deformation of the samples. The strain observed for approximately 10 min during the loading phase, which is considered to be of elastoplastic origin, has already been eliminated from the values for total strain.

The creep curves show a strongly overlinear increase of the creep strain in relationship to the vertical stress σ (Figures 3 and 4). Furthermore, it can be seen from the curves that an initially relatively large creep strain occurred over a short period directly after the load step. The increase in the creep strain then dropped steadily in the following days.

Consideration of the creep rate $\dot{\epsilon}^v$ allows a more detailed understanding of the creep behavior. It can be seen that directly after the load step, a very high creep rate occurs initially, then drops rapidly, reaching a more or less constant value after approximately 20 days. Sharp steps in the curves that can sometimes be observed at relatively low creep rates (in the range of $\dot{\epsilon} \leq 3 \cdot 10^{-7}$ 1/h) are not only due to the effects of small temperature changes, but also to the measuring method used: with a measuring accuracy of 10^{-3} mm and a minimum sampling frequency of 2/d, determined by the multi-channel recorder used, the deformation that takes place in the thus predetermined time interval of 12 h are of the same order as the maximum resolution of the measuring system. For this reason, it is planned to modify the measurement system in the future, so that instead of deformation being measured in a pre-determined time interval, the total time that is required for a pre-determined degree of deformation is measured.

In addition to the creep strain and the creep rate, Figures 3 and 4 also show the estimated minimum creep rate for each of the load steps. The minimum creep rate is considered to be due to secondary creep. Because of the occasional steps in the curves, the so-determined values for secondary creep rates must be considered with a degree of reserve.

In order to allow further evaluation, it was first necessary to resolve the continuously measured, three-stage creep tests with step-wise load increase into three individual tests at constant load. In order to do this, it was assumed that the total strain due to transient creep in each load step results from the additive superposition of the transient creep strain component of the previous load steps and that of the present load step (Figure 5 illustrates the method used).

As a simplification, it was assumed that the transient creep phase of the previous load step was already finished at the start of the new step. This condition is reached when the creep rate reaches the minimum value $\dot{\epsilon}^v_s$. In the case of tests where each load cycle is of extended duration, and the secondary creep has reached a constant minimum value, the time when the transient creep phase has just finished must first be determined. The transient creep component due to load step i can then be determined from the total creep strain $\epsilon^v(t)$ at this time with the help of the relationship

$$\epsilon^v_{tr,i} = \epsilon^v(t) - \dot{\epsilon}^v_{s,i} \cdot (t - t_{sc,i}) - \epsilon^v_{s,i-1} \qquad (6)$$

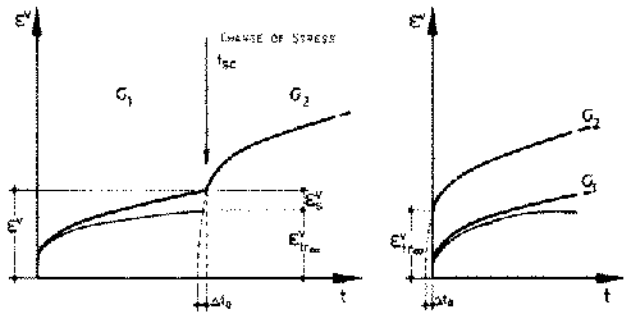

Figure 5. Resolution of multi-stage deformation tests into individual tests at constant load (example).

where

$\epsilon^v_{tr,i}$ = transient creep strain component due to load step i
$\epsilon^v(t)$ = total creep strain at time t
$\dot{\epsilon}^v_{s,i}$ = secondary creep rate due to load step i
$t_{sc,i}$ = time point of stress change (load step i)
$\epsilon^v_{s,i-1}$ = secondary creep strain due to all previous load steps 1 to i − 1.

In accordance with the material law Formulations (3) – (5), the above assumes that the transient and secondary creep components always combine additively.

In the case of the second and third load steps, it can be seen that in addition to the transient creep component due to the present load step, it is also necessary to estimate the time point of the start of the test (Δt_0, in Figure 5). In order to do this, it was assumed that the transient creep can be approximated by a KELVIN model (Herrmann, Wawersik and Lauson, 1980):

$$\epsilon^v_{tr} = \epsilon^v_{tr\infty}[1 - \exp(-\xi \cdot t)] \tag{7}$$

where

$$\epsilon_{tr\infty} = \sigma_1/\bar{G}_K \tag{7a}$$

$$\xi = G_K/\eta_K \tag{7b}$$

For the $\epsilon^v - t_i$ coordinate system of the i-th load step, it is then necessary to determine the time $t = \Delta t_{0,i}$ when the transient creep strain has reached the value $\epsilon^v_{tr\infty,i-1}$. In order to do this, the limiting conditions:

$$t = \Delta t_{0,i} \rightarrow \epsilon^v_{tr,i} = \epsilon^v_{tr\infty,i-1}$$

are inserted into Equation (7)

$$\epsilon^v_{tr\infty,i-1} = \epsilon^v_{tr\infty,i}[1 - \exp(-\xi_i \cdot \Delta t_{0,i})] \tag{8}$$

and then solved for $\Delta t_{0,i}$:

$$\Delta t_{0,i} = -\frac{1}{\xi_i} \cdot \ln\left(\frac{\epsilon^v_{tr\infty,i} - \epsilon^v_{tr\infty,i-1}}{\epsilon^v_{tr\infty,i}}\right) \tag{9}$$

The viscosity parameters G_K and η_K can then be determined from the relationships:

$$\bar{G}_K = \sigma_1/\epsilon^v_{tr\infty} \tag{10}$$

$$\eta_K = G_K \cdot t/\ln\left(\frac{\epsilon^v_{tr\infty} - \epsilon^v_{tr}}{\epsilon^v_{tr\infty}}\right) \tag{11}$$

Note that time t must include the component Δt_0. Since the shape of the creep curves shows that Δt_0 is relatively small for the tests under consideration, it was approximated to $\Delta t_0 = 0.2$ d for all load steps.

With the help of the assumption just outlined, the individual creep curves are thus resolved from the three-stage deformation tests with a step-wise load increase (for stresses of $\sigma = 12$, 14, 16, 18 and 20 MPa), as seen in Figure 6. Creep curves determined in this way were then used to determine the material parameters for each of the five Material Laws quoted previously. The following only describes the general method. More details are contained in Junge (1983).

PARAMETER DETERMINATION

Preparation

Material Laws 1–4 express the stress-dependency of the creep rate as a power law. Investigations on the creep mechanisms responsible for the macroscopic creep strain indicate that at a stress of $\sigma_v = 16$ MPa the dominant deformation mechanism changes from dislocation climb to dislocation glide (Albrecht and Hunsche, 1980). However, only a power law is suitable for dealing with dislocation climb.

A value for the stress exponent of $n = 6.5$ was determined from the secondary creep rate curves for the entire stress range from $\sigma = 12$ to 20 MPa. However, a separate determination for the stress range from $\sigma = 12$ to 16 MPa and from $\sigma = 16$ to 20 MPa indicated values for the stress exponent of $n = 4.92$ and $n = 9.28$, respectively. Thus, the generally accepted value of $n = 5$ is appropriate for the stress range below 16 MPa, whereas a considerably larger value should be used for stresses above 16 MPa. For this reason, only the stress range from $\sigma = 12$ to 16 MPa will be considered in the following discussion. Furthermore, a value for the stress exponent of $n = 5.0$ will be assumed for all material laws.

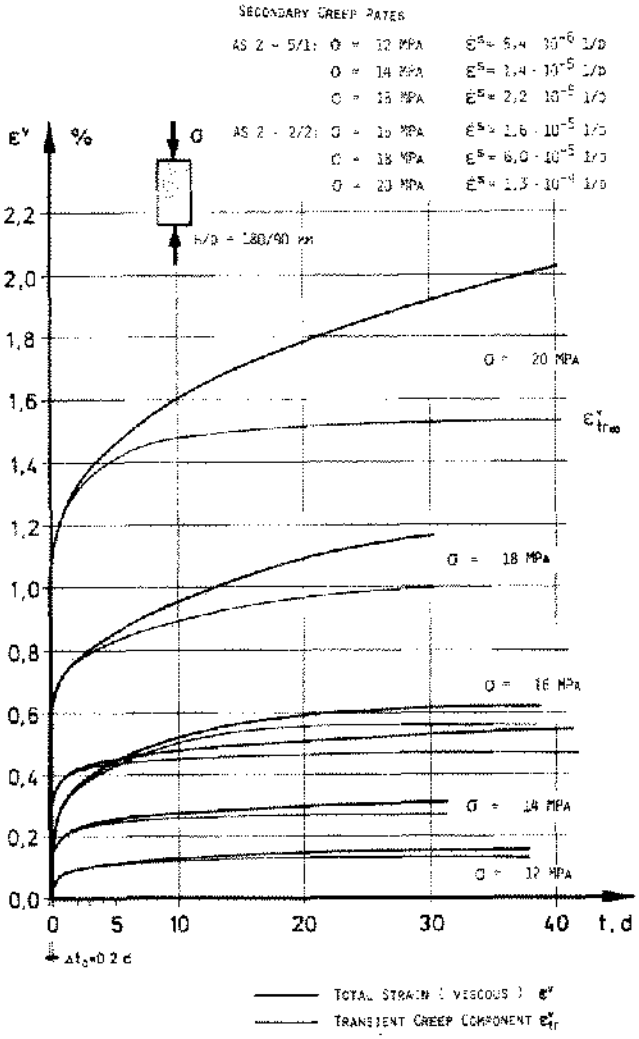

Figure 6. Resolved single-stage creep tests.

Material Law According to Boresi/Deere

In accordance with Equation (1), the Material Law from Boresi/Deere requires determination of the stress exponent n, the time exponent m and a pre-factor a. The stress exponent has already been pre-defined above (n = 5.0). The parameters m and a can then be determined for the three load steps from the relationship:

$$\epsilon^v = a^* \cdot t^m \tag{12}$$

with

$$a^* = a \cdot \sigma^{5.0}. \tag{12a}$$

The parameters a* and m can then be calculated from the pairs of values (t/ϵ^v) for the individual creep curves via potential regression analysis. a^* was then converted to a with the help of Equation (12a). The results were then averaged to obtain the final parameters, which were:

$$a = 3.9 \cdot 10^{-9} \text{MPa}^{-5} \cdot \text{d}^{-0.12};\ m = 0.12;\ n = 5.0$$

Material Law According to Menzel/Schreiner

It can be seen from Equation (2) that it is necessary to determine the parameters a*, n* and μ. They can be directly calculated from the parameters already determined for the Material Law from Boresi/Deere (Menzel and Schreiner, 1977):

$$\mu = \frac{1}{m} - 1 = 7.33$$

$$n^* = n \cdot (\mu + 1) = 41.67$$

$$a^* = \frac{1}{\mu + 1} a^{\mu - 1} = 1.011 \cdot 10^{-71} \text{MPa}^{-41.67} \cdot \text{d}^{-}$$

Material Law According to Odqvist/Hult

Equation (3) shows that it is necessary to determine the stress exponent n, the pre-factor a and the stress-dependent strain component due to transient creep. The stress exponent has already been determined (n = 5.0). The pre-factor can then be obtained from the relationship

$$a = \frac{\dot{\epsilon}^s}{\sigma^n} \tag{13}$$

using the secondary creep rates quoted in Figure 6. Equation (13) indicates an average value for the pre-factor a of $a = 2.29 \cdot 10^{-}$ MPa$^{-5.0} \cdot$ d^{-}. The following power law was then chosen for the transient creep component:

$$\epsilon^v_{tr\infty} = a^* \cdot \sigma^{n^*}. \tag{14}$$

For the stress range from σ = 12 to 16 MPa, regression analysis of the pairs of values $(\sigma/\epsilon^v_{tr\infty})$ indicated a value for the exponent of n* = 4.5. The average pre-factor a, determined via the relationship

$$a^* = \epsilon^v_{tr\infty} / \sigma^{n^*} \tag{14a}$$

was $a^* = .79 \cdot 10^{-6}$ MPa$^{-4.5}$.

Material Law According to McVetty/Hunsche

Equation (4) shows that the Material Law from McVetty/Hunsche requires the determination of a total of 7 parameters. The activation energies Q_1 and Q_2 can only be determined by tests at different temperatures. A value for Q_1 =

$Q_2 = 14.6$ kcal/mol $= 6.117 \cdot 10^4$ J/mol, as determined by Heusermann (1983) from temperature change tests on the same material, was used. According to Albrecht and Hunsche (1980), it can be assumed to a good approximation that Q_1 and Q_2 have the same value. Since this material law, too, expresses the stress-dependency of the creep rate with a power law, the stress exponent of the secondary creep rate has been set to $n_2 = 5.0$. The stress exponent for the transient creep rate corresponds to the value previously determined above, i.e., $n_1 = n^* = 4.5$. The parameters a and b can be simply determined by comparing the coefficients with the pre-factors determined for the material law from Odqvist/Hult. However, Equations (3b) and (4b) should be used for this purpose. This indicates that the parameter $a = 1.524$ MPa$^{-5.0} \cdot$ d^{-}, and $b = .9 \cdot 10^{-3}$ MPa$^{-4.5}$.

Finally, the parameter m must be determined. A comparison with the Material Law LUBBY 2 shows that the decay behavior of the transient creep rate can be expressed by the same exponential law. The parameter m is thus

$$m = \frac{G_K}{\eta_K}. \tag{15}$$

The parameters G_K and η_K were determined in the next section. Evaluation of Equation (15) for the stress range $\sigma =$ 12 to 16 MPa yields an average value $m = 0.5$ d^{-}.

Material Law LUBBY 2

Equations (5a)–(5c) assumes that the stress-dependence of the creep rate can be expressed as an exponential law, and thus the required parameters can be determined for the entire stress range from $\sigma = 12$ to 20 MPa. All unknown parameters in the following equations must be determined:

$$\bar{\eta}_M = \bar{\eta}^*_M \cdot e^{m \cdot \sigma} \tag{15a}$$

$$\bar{G}_K = \bar{G}^*_K \cdot e^{k_1 \cdot \sigma} \tag{15b}$$

$$\bar{\eta}_K = \bar{\eta}^*_K \cdot e\, k_2 \cdot \sigma. \tag{15c}$$

The parameters $\bar{\eta}^*_M$ and m in Equation (15a) can be directly determined from an exponential regression analysis of the pairs of values $(\sigma/\bar{\eta}_M)$. The Maxwell viscosities $\bar{\eta}_M$ can be obtained from the secondary creep rates quoted in Figure 6 via

$$\bar{\eta}_M = \frac{1}{\dot{\epsilon}^s_v}\,\sigma. \tag{16}$$

Regression analysis then indicates:

$$\bar{\eta}^*_M = 1.21 \cdot 10^6 \text{ MPa} \cdot \text{d};\ m = -3.27 \cdot 10^{-1}\ 1/\text{MPa}.$$

In order to determine the parameters $\bar{G}^*_K$ and k_1 in Equation (15b), it was first necessary to determine the stress-dependent Kelvin moduli $\bar{G}_K$. They can be obtained from the relationship

$$\bar{G}_K = \frac{\sigma}{\epsilon^v_{tr\infty}} \tag{17}$$

where the corresponding total transient strain $\epsilon^v_{tr\infty}$ can be obtained from Figure 6. The required parameters can then be determined via exponential regression analysis:

$$\bar{G}^*_K = 1.88 \cdot 10^5 \text{MPa};\ k_1 = -2.54 \cdot 10^{-1}\ 1/\text{MPa}.$$

In order to determine the parameters $\bar{\eta}^*_K$ and k_2 in equation (15c), it was first of all necessary to determine the stress-dependent Kelvin viscosity moduli $\bar{\eta}_K$. They can be obtained from equation (11), after inserting the pairs of values (t/ϵ^v_{tr}) for the individual creep curves, obtained from Figure 6. The respective average values $\bar{\eta}_K(\sigma)$ were then used in an exponential regression analysis, yielding the values:

$$\bar{\eta}^*_K = 4.98 \cdot 10^5 \text{ MPa} \cdot \text{d};\ k_2 = -2.67 \cdot 10^{-1}\ 1/\text{MPa}.$$

However, solely considering the stress-dependency of the Kelvin viscosity moduli does not allow a satisfactory description of the shape of the creep curves, particularly at the start of transient creep. According to Heusermann, Lux and Rokahr (1982) it is also necessary to consider the time-dependency of the Kelvin viscosity moduli. It can be described by a power law of the form

$$\bar{\eta}_K(\sigma,t) = \bar{\eta}'_K \cdot t^m \tag{18}$$

with

$$\bar{\eta}'_K(\sigma) = \bar{\eta}^*_K \cdot e^{k_2 \cdot \sigma}. \tag{18a}$$

The time-dependent Kelvin viscosity moduli $\bar{\eta}_K(t)$ were determined for each test. The parameters $\bar{\eta}'_K$ and m can then be determined by potential regression analysis. Tests AS 2 - 2/2 and AS 2-5/1 indicate an average value for the time exponent of $m = 0.66$.

The individual values lay in the range $m = 0.59$ to 0.74. The stress-dependence of the Kelvin viscosity moduli can be expressed via equation (18a). The parameters $\bar{\eta}^*_K$ and k_2 can be determined with the help of exponential regression analysis from the stress-dependent $\bar{\eta}'_K$ values. Regression analysis then yielded the following values:

$$\bar{\eta}^*_K = 2.51 \cdot 10^5 \text{ MPa} \cdot \text{d};\ k_2 = -2.85 \cdot 10^{-1}\ 1/\text{MPa}$$

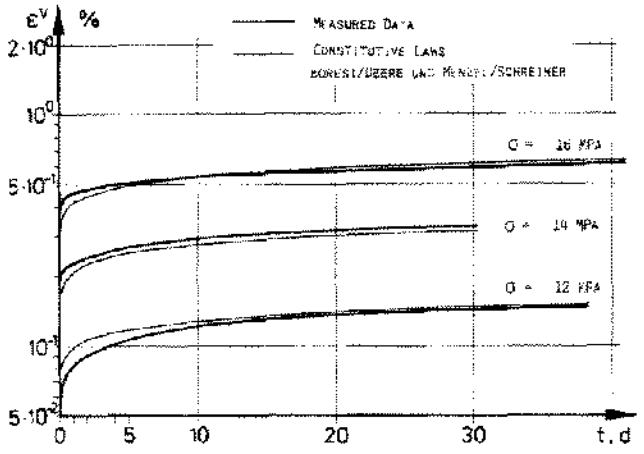

Figure 7. Comparison of measured and calculated creep strain.

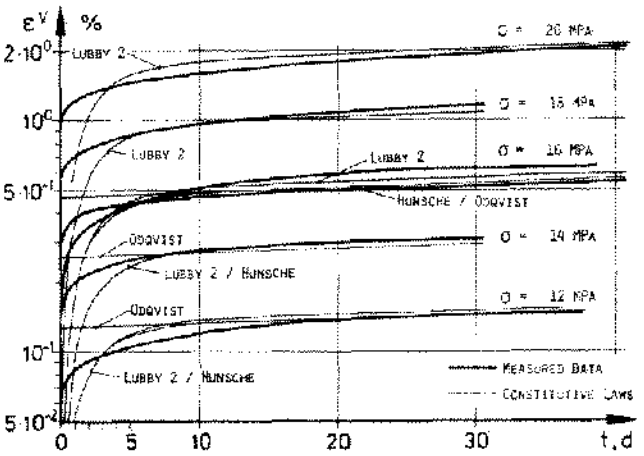

Figure 8. Comparison of measured and calculated creep strain.

SIMULATION OF LABORATORY TESTS

Comparison of Calculated and Measured Creep Behavior with Constant Load

With the help of the material parameters determined in the previous section (Equations 12 through 18) the creep behavior, as calculated from the various material laws, may be compared with the measured creep behavior obtained from the deformation tests, whereby Figures 7 and 8 compare the creep strains ϵ^v. It can be seen that apart from the initial part of the curve directly after the load step, all theoretical material laws are able to satisfactorily describe the creep strain measured in the laboratory. This is particularly true of the Material Law LUBBY 2, which covers a strain range of $\sigma = 12$ to 20 MPa.

The Material Laws according to Boresi/Deere and Menzel/Schreiner also yield good results in the initial curve region. The Material Law LUBBY 2 can be considerably improved by including a time-dependent component for the Kelvin viscosity modulus (see Equation (18)). No particular preference can be seen for any of the material laws, even if the creep rates illustrated in Figure 9 are compared. However, Figure 9 shows even more clearly that the Material Laws from Boresi/Deere and Menzel/Schreiner, which indicate identical creep rates and/or creep strains under constant load conditions, are best able to describe the decrease in creep rate and thus the creep behavior in the initial region. However, when considering longer time durations, this initial region is only of minor importance.

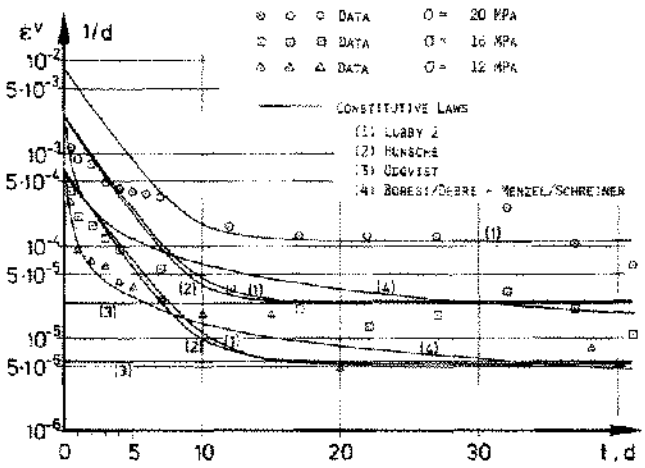

Figure 9. Comparison of measured and calculated creep rates.

Extrapolation to Longer Times

Significant differences in the calculated creep behavior, however, are indicated if an extrapolation to times longer than the test duration of approximately 40 days is undertaken. The creep strain for up to 2000 days for stresses of

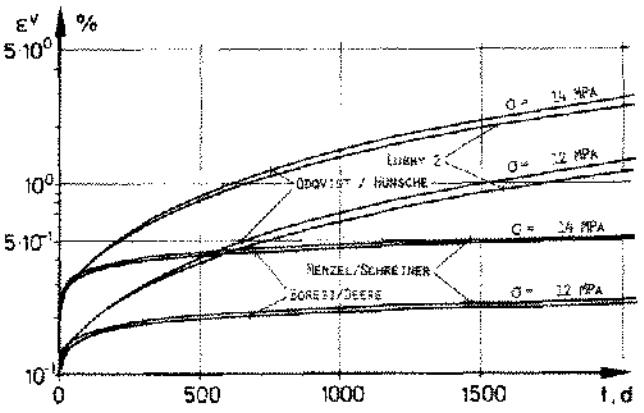

Figure 10. Extrapolation of creep strain to longer time periods—comparison of various formulations.

σ = 12 MPa and 14 MPa are shown in Figure 10. While on the one hand the Material Laws from Boresi/Deere and Menzel/Schreiner indicated in principle identical results (although small deviations are apparent in the curves as a result of numerical iteration), and on the other hand the Material Laws from Hunsche, Odqvist and LUBBY 2 also yielded similar results following extrapolation, the two sets differed considerably. This indicates, for example, values for the creep strain of ϵ^v = 0.23% and 1.1%, respectively, at a stress of σ = 12 MPa. The corresponding calculated creep rates vary by a factor of approximately 10. These considerable differences are related to the respective theoretical bases of the formulations: whereas the Material Laws from Boresi/Deere and Menzel/Schreiner assume a continuous hardening, leading to a continuous decrease in the creep rate, the other material laws assume the additive superposition of a transient creep component with decreasing creep rate and a secondary creep component with constant creep rate. The fact that Figure 9 shows similar creep rates for all formulations, particularly toward the ends of the curves, is due to the method used to determine the parameters which is related to the actual test duration. However, following extrapolation, the creep rate reduces still further for the formulations assuming hardening, whereas with the other formulations the creep rate remains nearly constant, thus leading to a considerably greater increase in the creep strain.

Comparison of the Calculated and Measured Creep Behavior for Multi-Stage Tests with Step-Wise Stress Increase

Further differences become clear when the formulations are used to predict the creep behavior with step-wise change in stress. This has already been mentioned by Penny/Mariott (1971). The results of the theoretical calculation of the step-wise stress increase tests AS 2-2/2 are shown in Figures 11 and 12. The test data are shown in Figure 3.

The creep strain and creep rates predicted with the Material Laws from Boresi/Deere and Menzel/Schreiner are shown in Figure 11. In particular, this figure clearly shows the qualitative difference between the assumption of time hardening and the assumption of strain hardening. In the former case, it is assumed that hardening is dependent on the total elapsed time. Following a stress change at time t_1 from stress σ_1 to stress σ_2, formulations based on time hardening predict the same creep rate at times $t > t_1$ as that due to a constant load test with a stress σ_2 at the same time t. The creep rate is thus already strongly reduced by the hardening, which is dependent on the total elapsed time. The increase of the creep strain after the load change is thus small. Therefore, the observed increase in transient creep following the load increase is incorrectly described. In contrast to this, the assumption of strain hardening leads to a renewed strong increase in the transient creep after the load

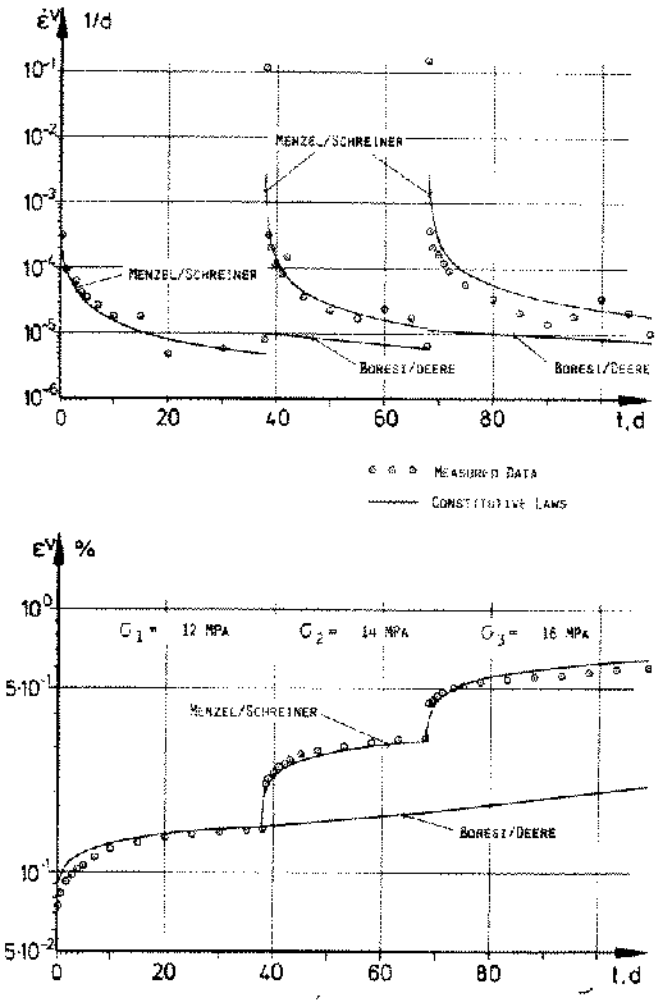

Figure 11. Calculated and measured creep behavior for multi-stage tests.

step, because in this case, the creep rate is dependent on the total creep strain up to that point. Following a load increase from σ_1 to σ_2 at the time t_1, the creep rate at time point $t > t_1$ is thus the same as that indicated by the creep strain for the higher stress σ_2 at the time point of the load change.

A comparison with the measured values for creep rate and creep strain shows that following the first load step, the assumption of time hardening does not lead to a good correlation between the calculated and measured creep behavior, whereas the assumption of strain hardening does yield a good correlation, both for the creep rate and for the creep strain.

For the purposes of comparison, Figure 12 shows the creep behavior calculated with the other material laws. Due to the secondary creep component, which is considered in the same way in all material laws, the creep rates show good correlation, with the exception of the transient creep region. However, the creep strain does not always correlate with the laboratory measurements, because the

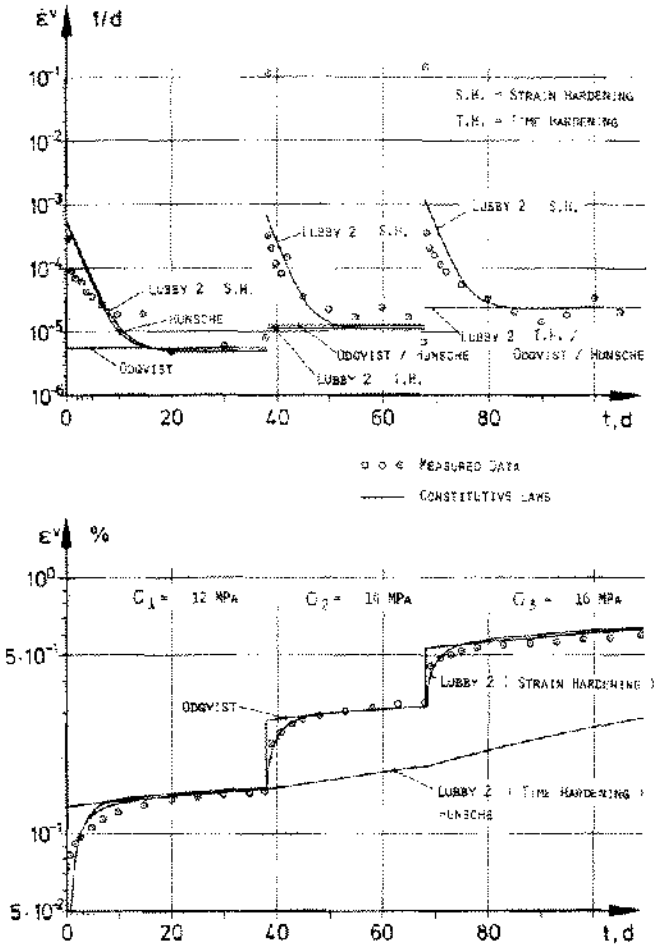

Figure 12. Calculated and measured creep behavior in multi-stage tests.

transient creep component still dominates in the time scale under consideration.

As with the Material Law from Boresi/Deere, the Material Law from Hunsche, which similarly assumes time hardening for the transient creep behavior, also indicates a value that is too small for the creep strain after the first load step: although the latter formulation indicates a higher value than in the Formulation from Boresi/Deere, because it also contains a component for secondary creep, the indicated creep strain is still much too small. The same is true for the Material Law LUBBY 2, under the assumption of time hardening, which yields practically identical results, despite the different assumption for the stress dependency. Although the Material Law from Odqvist does not yield a good correlation with the measured creep rates in the transient creep region, the creep strain is generally very well described, because the transient creep component is considered for each load step.

The best correlation with the laboratory measurements was obtained with the Material Law LUBBY 2 under the assumption of strain hardening (Equation (5b)). Both the change in the creep rate and the change in the creep strain are well described. The advantages of the initially phenomenologically-developed strain hardening theory, which became apparent during the comparitive investigations, can also be justified with the help of dislocation theory (Langer, 1980).

Generally speaking, it appears that only material laws which assume strain hardening are suitable when simulating the effects of stress increases. However, when extrapolating this conclusion to long-term convergence calculations, it should be remembered that the transient creep component continuously decreases in importance in comparison to the secondary creep component, and thus consideration of transient creep in the case of long time durations has only a low significance. In contrast to this, when simulating field tests of a relatively short duration, the transient creep has a considerably greater effect.

Multi-stage Tests with Step-wise Stress Decrease

Because, under *in situ* conditions, not only stress increases but also stress decreases can occur, e.g., in the case of an increase of the internal pressure in a cavity, it is also important to know how the rock salt behaves under such a load history, and to investigate the accuracy of correlation between the calculated and measured creep behavior. Penny/Mariott (1971) quote qualitative information on the behavior of various material laws with decrease in stress. The first investigations specifically dealing with rock salt were carried out by Herrmann/Lauson (1981). In addition to this, Hunsche (1981) and Heusermann (1982) have investigated the theoretical determination and interpretation of the creep behavior observed with rock salt in laboratory tests with step-wise load decrease. Most of the creep tests were two-stage, where a stress of σ_1 during the first stage was reduced to σ_2 in the second stage. For example, Hunsche (1981) describes the strain ε^v resulting from a stress change from $\sigma_1 = 12$ MPa to $\sigma_2 = 8$ MPa. The results are shown in Figure 13.

It can be seen that, following the load decrease, the creep rate soon reaches a value which remains practically constant over the relatively long test duration of approximately 200 days. Furthermore, the creep rate observed was considerably lower than the secondary creep rate to be expected for a stress of $\sigma_2 = 8$ MPa. This very surprising result, which is contradictory to expectations, is not indicated by the material laws discussed above. For this reason, Hunsche (1982) assumes that a stationary creep situation occurs directly after a load decrease to a new stress σ_2, with a constant creep rate that is considerably lower than that attained following a load increase to the same stress σ_2. Although this hypothesis appears initially plausible, it has a disadvantage in that the secondary creep rate, both in laboratory measurements and also theoretically, is dependent

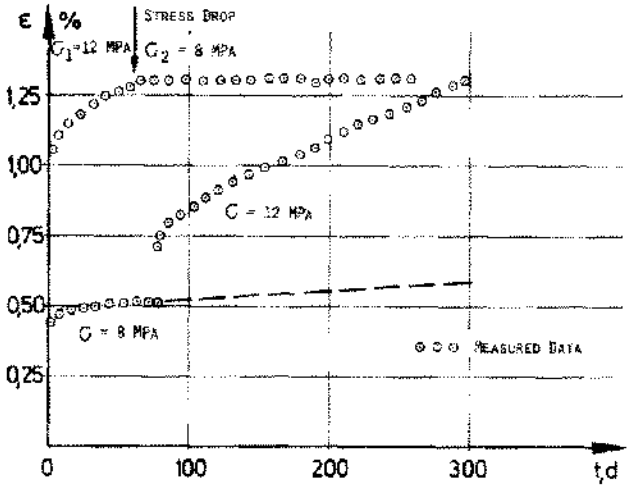

Figure 13. Multi-stage test with stress reduction, from Hunsche (1981).

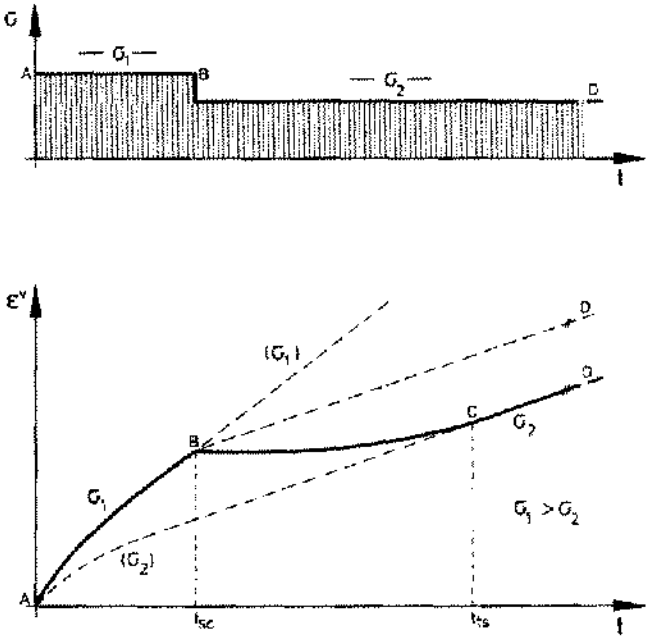

Figure 14. Two-stage creep test with stress reduction (example) above: applied stress, below: resulting creep strain.

on the prior load history—a consequence that contradicts the interpretation of stationary creep via the theory of dislocation mechanisms.

Herrmann/Lauson (1981) and Heusermann (1982) thus assume that the load history has no influence on the secondary creep rate related to a particular stress level. Furthermore, it is assumed that by analogy to the method used to interpret creep tests with step-wise load increase, in the case of load decrease too, the total creep rate $\dot{\epsilon}^v$ can be separated into two additive components. However, in contrast to the tests with stress increase, the transient creep component $\dot{\epsilon}^v_{tr}$ should be set negative in sign, whereas the secondary creep component remains positive as before, in order to reflect the results of laboratory measurements, which show that the creep rate directly after the load reduction is initially much less than the secondary creep rate corresponding to the new stress level σ_2. Accordingly:

$$\dot{\epsilon}^v(t \geq t_{sc}) = -\dot{\epsilon}^v_{tr} + \dot{\epsilon}^v_s. \qquad (19)$$

The following analysis considers a two-stage creep test with a stress level of σ_1 in the first stage and a stress reduction of σ_1 to σ_2 in the second stage. Figure 14, which shows, in addition to the applied stress $\sigma(t)$, the qualitative change in the creep strain ϵ^v with time, is based on the limited laboratory data available, as interpreted by Equation (19) with respect to the sign of the transient creep component. Following the stress decrease to σ_2 at point B (time $t = t_{sc}$), curve section BC, with increasing creep rate, can be considered to be transient creep. A constant secondary creep rate $\dot{\epsilon}^v_s$ is then attained at time $t = t_{ts}$, the corresponding creep strain being related to the new stress σ_2 (curve section CD).

Assuming, in principle, a continuous additive superposition of transient and secondary creep as expressed in Equation (19), the material laws expressed in Equations (3), (4) and (5) can also be used to describe the creep behavior following load decrease after changing the sign of the transient creep component, since they are based on the same fundamental idea, although they were developed from tests with step-wise load increase. However, formulations based on time hardening for the transient creep component have the disadvantage that, even for a solely qualitative agreement with the observed creep behavior following the load decrease, they require the introduction of a new local coordinate system with origin corresponding to the timepoint t_{sc} of the load step. This is necessary in order to eliminate the additive effects of material hardening which has taken place prior to that point in time. However, an assumption of this nature contradicts fundamental considerations relating to dislocation theory, and is solely based on empirical considerations.

For this reason, in the following, the creep behavior following the load step will be described solely with Material Law LUBBY 2 (Equation (5b)), which is based on strain hardening for the transient creep component. In conjunction with Equation (19), and for the case of uniaxial stress, the creep behavior following load decrease can then be described in the following way:

$$\dot{\epsilon}^v(t \geq t_{sc}) = \left[-\frac{1}{3\eta^D_K(\sigma)} \cdot \left(1 - \frac{\bar{\epsilon}^v_{tr}}{\sigma} \cdot 3G^D_K(\sigma)\right) + \frac{1}{3\eta^D_M(\sigma)} \right] \cdot \sigma, \qquad (20)$$

The material parameters contained in equation (20) are marked with an index 'D' (D = Decrease) to indicate that they are valid for the case of stress reduction. They should be so determined that the same equation can be used for both load decrease and load increase, simply by changing the sign of one of the components. First of all, the viscosity parameter η_M^D will be considered. Assuming that transient and stationary creep are additive, and assuming that the transient creep component becomes zero at the end of the transient creep phase (at $t = t_{ts}$), Equation (19) indicates that:

$$\epsilon^v(t \geq t_{ts}) = \dot{\epsilon}_s^v(\sigma). \tag{21}$$

Equation (20) then shows that the viscosity parameter η_M^D is:

$$\eta_M^D = \frac{1}{3\dot{\epsilon}_s^v} \cdot \sigma. \tag{22}$$

Furthermore, it is also assumed that the load history has no influence on the secondary creep rate, the latter being solely dependent on the current stress. Thus, $\dot{\epsilon}_s^v$ is identical to the secondary creep rate previously determined in multistage tests with step-wise stress increase. The Maxwell viscosity parameter is thus:

$$\bar{\eta}_M^D(\sigma) \equiv \bar{\eta}_M(\sigma) = \bar{\eta}_M^* \cdot e^{m\sigma} \tag{23}$$

with $\bar{\eta}_M^*$ and m as in Equation (15a).

The secondary creep component is thus identical for both stress increase and stress decrease. In contrast, the material parameters G_K^D and η_K^D, and the size and time-dependency of the transient creep component, are dependent on the previous load step. The transient creep phase BC in Figure 15 will now be simulated with three qualitatively different Formulations (I), (II) and (III), which are based on LUBBY 2. Figure 15 shows the creep strain ϵ^v and the associated creep rate $\dot{\epsilon}^v$.

Starting with the boundary conditions for the creep rate $\dot{\epsilon}^v$ and the creep strain ϵ^v at time $t = t_{sc}$ directly after the load step and at time $t = t_{ts}$ at the end of the transient creep phase (i.e., the beginning of the secondary creep phase), the parameters G_K^D and η_K^D will now be determined for each of the three formulations.

Formulation (I):

The simplest simulation of the creep range BC is achieved by ignoring the effects of transient creep. In this case, the creep rate immediately assumes a constant value corresponding to the secondary creep due to the new stress σ_2 directly after the load step. This is expressed in the following boundary condition:

$$t \geq t_{sc} \longleftrightarrow \dot{\epsilon}_{tr}^v = 0. \tag{24}$$

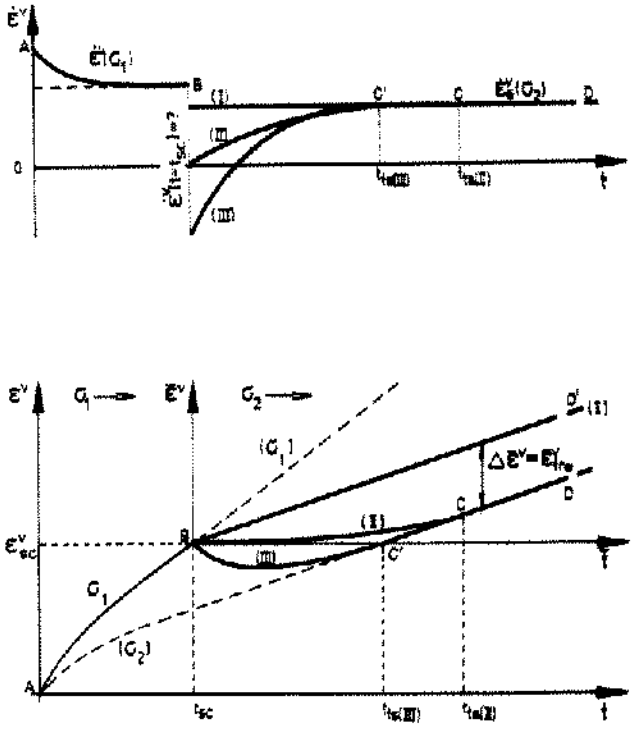

Figure 15. Two-stage creep test with stress reduction (example) Simulation with Formulations I, II, III (see text) above: creep rate, below: creep strain.

Inserting this boundary condition and Equation (23) into Equation (20) shows that:

$$\dot{\epsilon}^v = \frac{1}{3\eta_M(\sigma)} \cdot \sigma. \tag{25}$$

This corresponds to a creep strain which increases linearly with time (curve I in Figure 15b). It can be seen that the creep strain is overestimated in comparison to the measured behavior, and thus this formulation can be considered to represent the upper limit.

Formulation (IIa):

In this case, the theoretical creep rate is assumed to drop to zero directly after the load decreases at time $t = t_{sc}$, followed by a slow increase to the constant value $\dot{\epsilon}_s^v(\sigma_2)$ corresponding to the secondary creep due the new stress σ_2. The curve for creep strain (curve II in Figure 15b) thus initially has a horizontal tangent, followed by an increase until the creep strain corresponds to the measured secondary creep, at point C. Thereafter, both theoretical and measured creep are in agreement (curve section CD). This can be expressed in the following boundary conditions:

$$t = t_{sc} \longleftrightarrow \dot{\epsilon}^v = 0 \tag{26a}$$

$$t = t_{sc(II)} \longleftrightarrow \epsilon^v = \epsilon^v(\sigma_2). \tag{26b}$$

In conjunction with Equation (20) and whilst considering the boundary condition $\bar{\epsilon}^{v}_{tr}(t = t_{sc}) = 0$, Equation (26a) then indicates that the Kelvin viscosity modulus η^{D}_{K} is:

$$\eta^{D}_{K}(\sigma_2) = \eta_M(\sigma_2). \tag{27}$$

The second boundary condition, Equation (26b), can be used to determine the Kelvin shear modulus G^{D}_{K}. Just as with tests with step-wise stress increase, if $\bar{t} \rightarrow \infty$ then the Kelvin shear modulus can be obtained from:

$$\bar{G}^{D}_{K}(\sigma) = \frac{\sigma}{\bar{\epsilon}^{v}_{tr\infty}}. \tag{28}$$

With the help of geometrical interrelationships between the creep curves with constant stresses of σ_1 and σ_2, several transformations then indicate that:

$$\bar{G}^{D}_{K}(\sigma_2) = \frac{\sigma_2}{\left(1 - \frac{\sigma_2}{\sigma_1} \cdot \frac{\eta_M(\sigma_1)}{\eta_M(\sigma_2)}\right) \cdot \left(\epsilon^{v}_{sc} - \frac{\sigma_1}{3G_K(\sigma_1)}\right) + \frac{\sigma_1}{3G_K(\sigma_2)} - \frac{\sigma_2}{3G_K(\sigma_2)}} \tag{29}$$

where the Kelvin shear moduli $G_K(\sigma_1)$ and $G_K(\sigma_2)$ are obtained via Equation (17) from the transient creep component, due to the same stress level but for a stress increase. If the load step occurs at a time point where the transient creep phase is not yet ended, then $\epsilon^{v}_{tr\infty}$ should be replaced by the actual transient creep strain $\epsilon^{v}_{tr}(t_{sc})$ at that time point.

The initially-unknown time point $t_{ts(II)}$, which characterizes the end of the transient creep phase and/or the beginning of the secondary creep phase, can be obtained from a further boundary condition:

$$t = t_{ts(II)} \longrightarrow \dot{\epsilon}^{v} = \alpha \cdot \dot{\epsilon}^{v}_{s}. \tag{30}$$

Since, as shown in Equation (15b), the transient creep strain approaches the final value $\epsilon^{v}_{tr\infty}$ asymptotically, the time point when the transient creep phase is considered to be finished must be set by definition. It will be assumed in the following that the transient creep phase is finished when the creep rate reaches 95% of the secondary creep rate. Thus, Equation (30) should be set to $\alpha = 0.95$.

Formulation (IIb):

Formulation (IIb) is very similar to Formulation (IIa). However, to simplify Equation (29), it can be assumed that the transient creep components $\epsilon^{v}_{tr\infty}(\sigma_1)$ and $\epsilon^{v}_{tr\infty}(\sigma_2)$ are related to each other in the same way as the corresponding secondary creep rates $\dot{\epsilon}^{v}_{s}(\sigma_1)$ and $\dot{\epsilon}^{v}_{s}(\sigma_2)$. Equation (29) then becomes:

$$\bar{G}^{D}_{K}(\sigma_2) = \frac{\sigma_2}{\epsilon^{v}_{sc}\left(1 - \frac{\sigma_2}{\sigma_1} \cdot \frac{\eta_M(\sigma_1)}{\eta_M(\sigma_2)}\right)}. \tag{31}$$

In contrast to Equation (29), the Kelvin shear modulus prior to the stress reduction is now only dependent on the stress σ_1 prior to and the stress σ_2 following the load step, to the creep strain ϵ^{v}_{sc} at the time point of the stress step and on the Maxwell viscosity moduli $\eta_M(\sigma_1)$ and $\eta_M(\sigma_2)$.

Formulation (III):

As with the Material Law from Herrmann/Lauson (1981), which was specially formulated for rock salt, several of the general Material Laws from Penny/Marriott (1971) indicate a creep of reversed direction following a stress reduction, leading to a creep strain in opposite direction to the stress. This "recovery creep" disappears with time, the creep strain then approaching the creep strain expected for the new stress σ_2. However, a reversible creep of this type following a stress reduction is neither visible in the laboratory results documented by Herrmann/Lauson (1981) nor by Hunsche (1981). Because this behavior was also not observed in the course of the author's own laboratory investigations, no further discussion of Formulation (III) will be undertaken.

Consideration of the equations required to calculate the material parameters η^{D}_{M}, η^{D}_{K} and G^{D}_{K} required by Formulations (I), (IIa), and (IIb) shows that the parameters which describe the creep behavior following the stress reduction can be calculated from the corresponding parameters at the time point of the stress step. It is neither necessary to introduce a local coordinate system, nor does the prior load history have any influence on the creep behavior after the stress step.

The theoretical Formulations (I), (IIa), and (IIb) will now be compared with the measured creep behavior of rock salt. The measured creep strain and creep rate in a two-stage laboratory test are shown in Figure 16. A stress of $\sigma_1 = 20$ MPa was used in the first stage. It can be seen that the creep rate reached a constant value after aproximately 30 days. The stress reduction to $\sigma_2 = 16$ MPa then took place at $t = t_{sc} = 38$ days, leading to a strong decrease in the creep rate. In the following period up to the end of the tests at $t = 110$ days, the creep rate showed only a slight increase, reflected in a very small increase in the creep strain. No signs of "recovery creep" are present.

The test data illustrated in Figure 16 were then used to calculate the following material parameters:

$$\bar{\eta}^{D}_{M}(\sigma) = \bar{\eta}_{M}(\sigma) = 5.54 \cdot 10^{7} \cdot e^{-0.327 \cdot \sigma} \text{ (according to Equation 23)}$$

$$\bar{\eta}^{D}_{M}(\sigma_2 = 16\,\text{MPa}) = 2.96 \cdot 10^{5}\,\text{d MPa}$$

$\bar{\eta}_K^D \equiv \bar{\eta}_M^D = 2.96 \cdot 10^5$ d MPa (according to Equation 27)

$\bar{G}_{K(IIa)}^D = 8.71 \cdot 10^2$ MPa (according to Equation 29)

$\bar{G}_{K(IIb)}^D = 8.21 \cdot 10^2$ MPa (according to Equation 31)

The values for the Kelvin shear moduli $\bar{G}_K^D$ for Formulations (IIa) and (IIb) are virtually identical, and thus only small differences in the calculated creep behavior can be expected between these two formulations.

For the purpose of comparison, Figure 16 also shows the creep strain and creep rate calculated with the above parameters. It can be seen that in the transient creep phase following the load decrease, Formulation (I) overestimates both the measured creep rate and the measured creep strain. However, the percentage difference becomes smaller with increase in time, because the actual creep rate approaches the secondary creep rate corresponding to the new stress level. In contrast to this, Formulations (IIa) and (IIb) lead to a generally very good correlation with the measured data.

However, the measured data in Figures 16 and 13 do not show any significant increase in the creep rate toward the expected secondary creep rate $\dot{\epsilon}_s^v(\sigma_2)$, which might indicate that the secondary creep phase has not been attained, even for test durations of 100 or 200 days. It is thus of particular interest, at least from the theoretical point of view, to be able to estimate the duration of the transient creep phase on the basis of the above assumptions.

A duration of the transient creep phase of around 1000 days can be expected, assuming the transient creep phase is finished when the theoretical creep rate has reached 95% of the secondary creep rate corresponding to the new stress level σ_2 (Figure 17). In contrast, following the stress reduction at time $t_{sc} = 38$ days, laboratory measurements were only made for another approximately 70 days. It is thus clear that considerably greater timescales are necessary to confirm the material law formulated for the simulation of creep behavior following a stress reduction as expressed in Equations (19) and (20).

Clearly, the duration of the transient creep phase is also dependent on the stress σ_1 in the first stage of the test, and on the differential stress $\Delta\sigma = \sigma_1 - \sigma_2$. The values chosen above, $\sigma_1 = 20$ MPa and $\Delta\sigma = 4$ MPa represent relatively large values. The duration of the transient creep phase increases with increasing differential stress, as shown in Figure 18.

If $\sigma_1 = 20$ MPa is reduced to $\sigma_2 = 16$, 17, 18 and 19 MPa after the load step at $t_{sc} = 38$ days, the approximate dura-

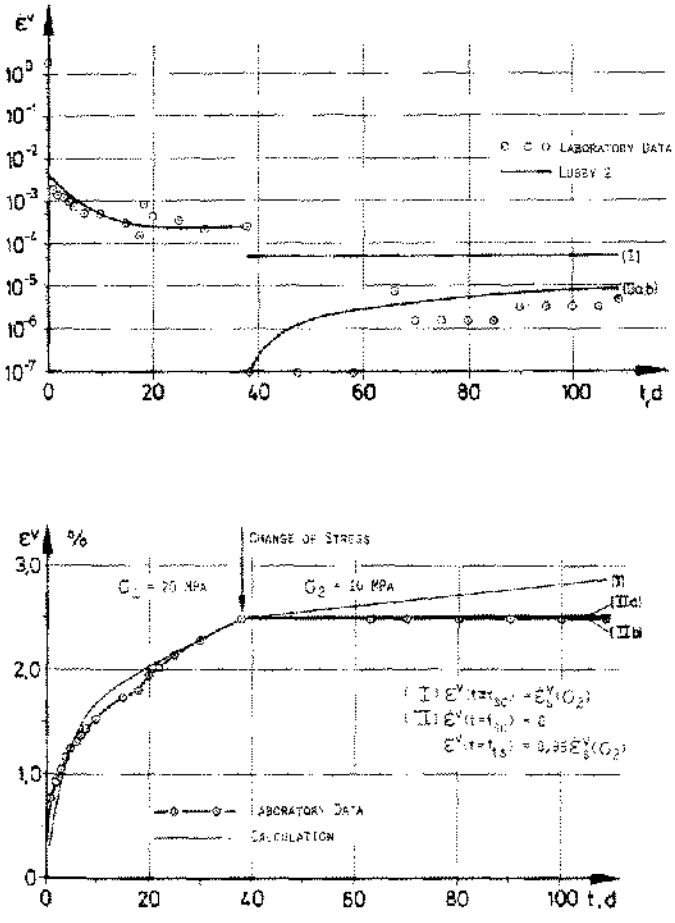

Figure 16. Two-stage tests with stress reduction—comparison of calculated and measured behavior.
above: creep rate below: creep strain

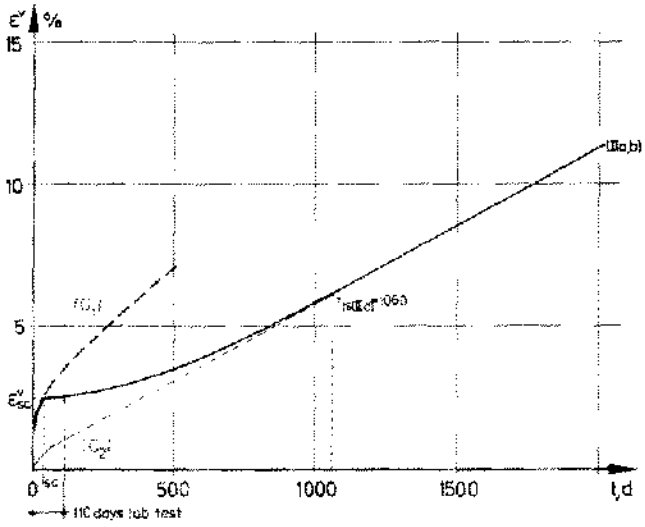

Figure 17. Estimation of the duration of the transient creep phase in the case of stress reduction from $\sigma_1 = 20$ MPa to $\sigma_2 = 16$ MPa (extrapolation).

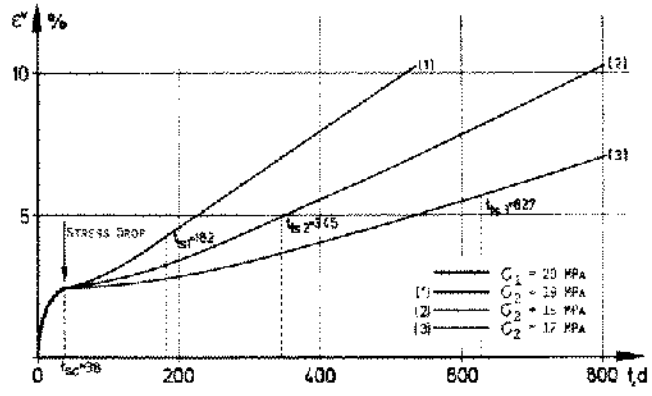

Figure 18. The influence of the differential stress on the duration of the transient creep phase.

tion of the transient creep phase after the load step becomes ~1020, ~590, ~305 and ~145 days, respectively. The time scales thus start to become very long for laboratory investigations. Furthermore, a differential stress of below 2 MPa can lead to resolution problems. A three-stage creep test with $\sigma_1 = 18$ MPa, $\sigma_2 = 20$ MPa and $\sigma_3 = 18$ MPa is currently being undertaken.

The duration of the transient creep phase is, however, not only dependent on the stress before and after the stress step, but also on the total creep strain ϵ^v_{sc} at the time of the stress step, which, in turn, is related to t_{sc}.

The theoretical creep behavior with a stress reduction from $\sigma_1 = 20$ MPa to $\sigma_2 = 19$ MPa for differing times t_{sc} of the load step, and thus differing creep strains ϵ^v_{sc}, is shown in Figure 19. It can be seen that with increasing ϵ^v_{sc} the duration of the transient creep phase also increases. In the case shown, a delay of 40 days in the load step leads to an increase in the duration of the transient creep phase following the load step from 105 days to 212 − 60 = 152 days. The influence of ϵ^v_{sc} on the duration of the transient creep phase is thus not so strong as the influence of the differential stress, but still significant.

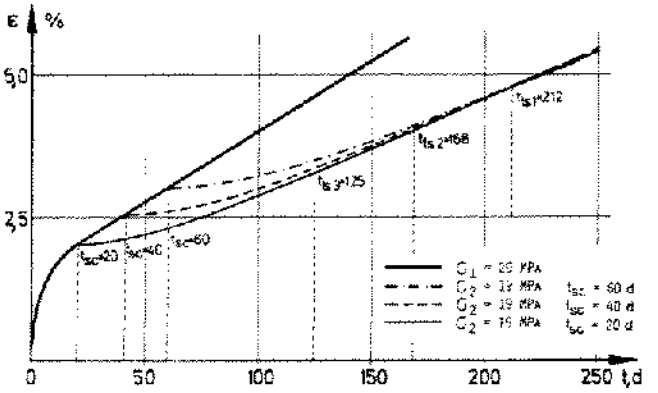

Figure 19. Influence of the time point of the load step on the duration of the transient creep phase.

To summarize, the best simulation of multi-stage creep tests with stress reduction was obtained with material laws that assume the additive superposition of a transient and a secondary component, where the transient creep component is based on strain hardening.

Creep Tests with Samples with an Axial Hole

The previous sections have shown that the theoretical simulation of uniaxial and triaxial creep tests under constant loads do not indicate any major preference for any of the five material laws investigated. On the contrary, for test durations of a few weeks or months, all material laws considered in the comparative investigation were able to satisfactorily describe the measured creep behavior, when one ignores slight differences in the initial transient creep directly after the load step. However, when extrapolating to longer time scales, qualitative differences become apparent and when simulating tests with stress steps, additional qualitative differences appear (See Comparison of Calculated and Measured Creep ... above). This indicates that in particular applications certain material laws are less suitable for fundamental reasons. Such differences could become significant, for example, if material laws based on time hardening are used to predict long-term convergence in the case of solution mining (with changing cavity geometry), or when investigating situations with changing load conditions.

First investigations of the creep behavior of models with stress reduction also showed substantial differences in the calculated creep deformation according to which material law is used (Lux/Rokahr, 1981), although the parameters of all material laws were determined from the same constant-load creep tests. Field measurements—e.g., convergence measurements in boreholes or measurements in storage caverns—offer little help here. This is because the measured convergence only allows an overall picture to be made of the deformation behavior of the structure, which is not only dependent on the material behavior and geometry of the structure, but on other factors such as the primary stress condition, the local geological situation and the temperature of the rock mass, factors which can only be estimated (Figure 20). Whilst the results of field measurements are suitable for a general confirmation of the usefulness of an integral design concept by comparison of, e.g., the measured and calculated convergence, they are not suitable to identify the advantages of any particular formulation in comparison to another, or to determine material parameters such as viscosity modulus. Due to the numerous boundary conditions involved, accurate simulation of the measured convergence does not offer a unique proof of the suitability of any one formulation, because in any specific situation the same results can often be obtained with different combinations of parameters (Heusermann, 1982).

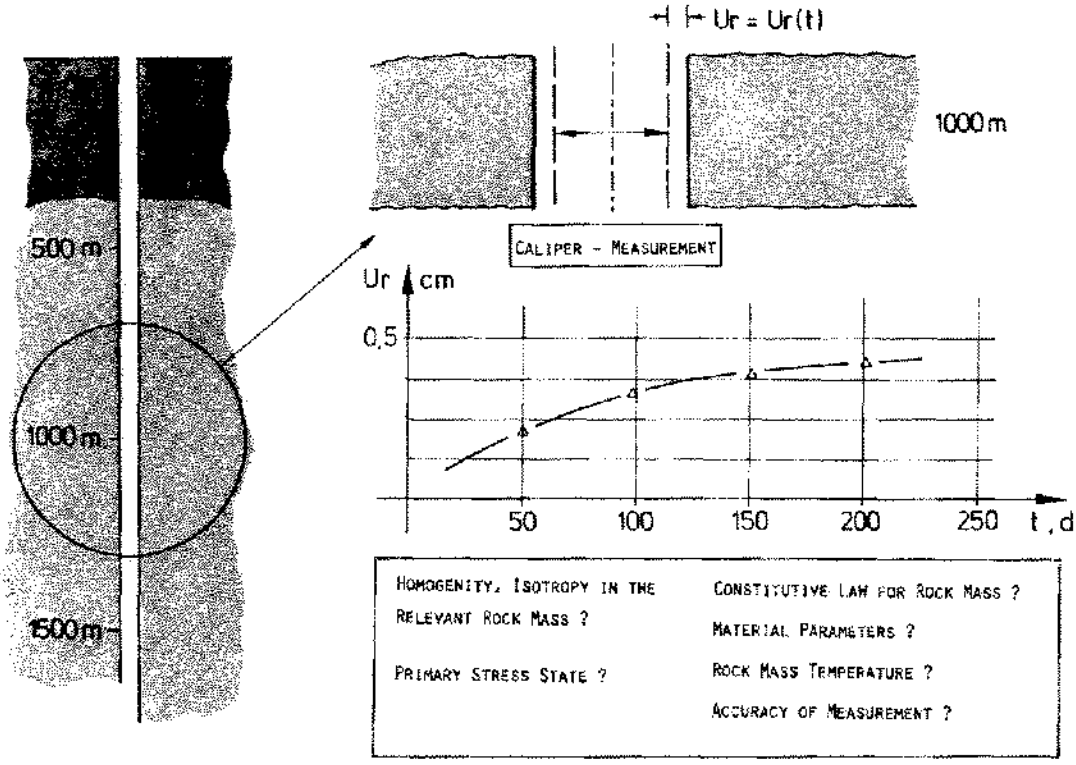

Figure 20. Additional factors which influence the measured data in the case of field tests.

It was hoped that the situation could be clarified with the help of laboratory tests on samples in which axial holes have been drilled. Such tests have already been used to determine the convergence behavior of caverns (Dreyer, 1973, Serata/Gloyna, 1960). However, in the present investigation, such tests were not used as the basis of model calculations whose results are to be transfered to the load-bearing capacity of an underground construction. Accordingly, a discussion of the mechanics of similitude will not be carried out here. The new, so-called LUBBY test method, which was proposed by Lux/Rokahr (1982), will be considered in just the same way as the other tests described in this paper, the difference lying solely in the geometry of the sample. Whereas tests with samples with axial holes also offer simple and clearly determinable geometric and stress conditions (hollow cylinder, external axial and radial pressure), they have one considerable advantage over the previous test series in that the changed geometry results in the appearance of viscous stress relaxation under stress. Despite the fact that the stress relaxations results from stress that is artificially applied to the exterior of the sample, its characteristics are solely dependent on the relaxation properties of the sample material and not on outside influences. In this way, it was hoped to obtain important additional confirmation of the validity of the material laws.

It is first necessary to determine the material parameters required for each material law from either uniaxial or triaxial creep tests with undrilled samples, as described in the section on Parameter Determination, above. The material laws were then used to simulate the results of creep tests carried out on samples of the same material but with axial holes, via triaxial compression and extension tests. A material law that is able to describe the stress relaxation behavior of rock salt by nature of its formulation, and has not just been adjusted to correlate to creep curves made under specific geometric and stress conditions, should also be able to simulate the results of tests with samples with axial holes using the same parameter values determined previously for undrilled samples. Without such a confirmation of a material law in the laboratory, its application in the considerably more complex situation in the field appears more or less meaningless, particularly in the case of the detailed interpretation of field measurements.

A sample with an axial hole whose creep behavior has been investigated under triaxial extension is shown in Figure 21. The measured vertical strain with an axial stress of 2 MPa and a confining stress of 16 MPa is illustrated in Figure 22, and it also shows the measured data obtained with an undrilled sample under the same deviatoric load conditions in uniaxial tests.

It can be seen that although the external deviatoric

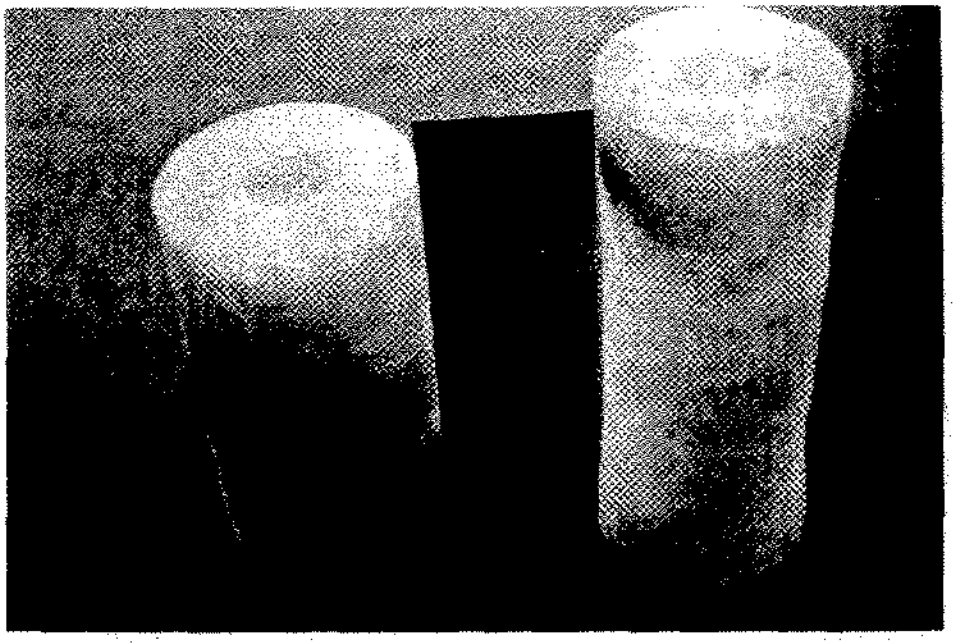

Figure 21. Test sample with axial drilled hole before and after triaxial extension tests.

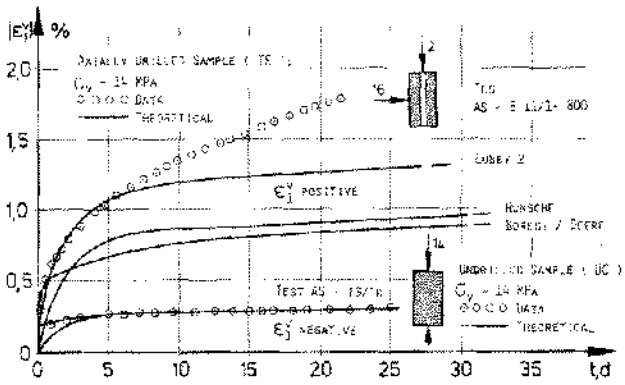

Figure 22. Comparison of measured and calculated creep strain for an undrilled and a drilled sample, with an external deviatoric stress of $\sigma_v = 14$ MPa.

stress is the same in both cases (14 MPa), the creep strain of the drilled sample is considerably larger than that of the undrilled sample. This difference in creep behavior, which is due to the differing internal stress condition within the sample, should also be indicated by the theoretical model.

Theoretical simulation of the creep tests was made with the help of the finite-element program UTROEPV. This program, which has been specially developed for the analysis of rotation-symmetrical continua with plastic and viscous material behavior, also allows calculation according to the three material laws expressed in Equations 1, 4 and 5b. In the case of the undrilled sample, and using the parameters determined above under Parameter Determination, it can be seen that the creep strain calculated with all three formulations is virtually identical and correlates well with the measured data (Figure 22).

As a comparison, the results of the theoretical simulation for the drilled sample are shown in Figure 22. It can be seen that although in qualitative agreement with the laboratory measurements, all formulations indicate a higher creep strain than for the undrilled sample, and marked differences between the predictions of the individual material laws become apparent within the time scale of the laboratory tests. The poorest agreement with the measured data, both qualitatively and quantitatively, was given by the formulation from Boresi/Deere, which indicated the lowest values for creep strain. The Material Law from Hunsche indicated only slightly higher values. However, the latter formulation indicated that additional creep takes place with more or less constant creep rate, whereas the formulation from Boresi/Deere, which is based on time hardening, predicts a continuous decrease of the creep rate, and thus an increasingly larger deviation from the measured values. The best agreement with the measured data was given with the Material Law LUBBY 2, especially in the transient creep phase. However, after about five days, here too, the predicted creep rate was substantially lower than the measured value, so, just as with the other formulations, the deviation between the predicted and the measured creep strain increases continuously with increase in time.

Although this initial simulation of a creep test with a sample having an axial hole did not lead to the identification of any one material law that is able to describe the

measured creep behavior with complete satisfaction, it can be seen that the LUBBY test is able to confirm in the laboratory, at least in principle, the suitability of a particular material law for the prediction of creep behavior. The marked differences in the predictions obtained with different formulations when treating more complex test structures (i.e., drilled samples) rather than undrilled samples indicates the importance of detailed investigations of the type described in this paper. Accordingly, it is planned to make further laboratory tests with other boundary conditions, followed by detailed numerical simulation.

REFERENCES

Albrecht, H. und U. Hunsche. 1980. Gebirgsmechanische Aspekte bei der Endlagerung radioaktiver Abfälle in Salzdiapiren unter besonderer Berücksichtigung des Fließverhaltens von Steinsalz. Fortschr. Miner. (58), H. 2, pp. 212–247.

Boresi, A. P. and D. U. Deere. 1963. Creep Closure of a Spherical Cavity in an Infinite Medium. Report for Holmes and Narver, Inc., Las Vegas, 82 pages.

Dreyer, W. 1973. Results of Recent Studies on the Stability of Crude Oil and Gas Storage in Salt Caverns. Proc. 4th Symp. on Salt, Vol. 2, pp. 65–92. The Northern Ohio Geological Society, Inc., Cleveland (Ohio).

Herrmann, W. and H. S. Lauson. 1981. Analysis of Stress Drop in Multistage Creep Experiments. Predictions of Exponential Creep Law. Sandia National Laboratories, SAND-81-1612. 18 pages.

Heusermann, S. 1982. Kritische Gegenüberstellung und Bewertung von Stoffgesetzen zur Beschreibung des Kriechverhaltens von Steinsalz. Forschungsergebnisse aus dem Tunnel— und Kavernenbau. Institut für Unterirdisches Bauen, Universität Hannover, Heft 6. 206 pages.

Heusermann, S., Lux, K. H. and R. B. Rokahr. 1982. Entwicklung mathematisch-mechanischer Modelle zur Beschreibung des Stoffverhaltens von Salzgestein in Abhängigkeit von der Zeit und von der Temperatur auf der Grundlage von Laborversuchen. Schlußbericht zum Forschungsvorhaben ET 2011 A, Institut für Unterirdisches Bauen, Universität Hannover. 434 pages.

Hunsche, U. 1981. Results and Interpretation of Creep Experiments on Rock Salt. Proc. 1st Conf. on the Mechanical Behavior of Salt, Penn State University, 8 pages.

Junge, A. 1983. Identifizierung von viskosen Stoffgesetzen anhand einaxialer Spannungswechselversuche. Diplomarbeit am Institut für Unterirdisches Bauen, Universität Hannover, 115 pages.

Langer, M. 1980. Das Verformungs—und Bruchverhalten von Steinsalz—Zusammenfassende Darstellung einiger Forschungsergebnisse der BGR zur Salzmechanik. Bundesanstalt für Geowissenschaften und Rohstoffe, Hannover. 62 pages.

Lux, K. H. 1984. Gebirgsmechanischer Entwurf und Felderfahrungen im Salzkavernenbau. F. Enke Verlag, Stuttgart. 357 pages.

Lux, K. H. and R. B. Rokahr. 1981. Laboratory Investigations and Theoretical Statements as a Basis for the Dimensioning of Caverns in Rock Salt Formations; Proc. 1st Conf. on the Mechanical Behavior of Salt, Penn State University, 36 pages.

Lux, K. H. and R. B. Rokahr. 1982. Einige Ergebnisse aus Laborversuchen zum mechanischen Verhalten von Steinsalz und ihre Bedeutung für den theoretischen Entwurf von Speicherkavernen. Proc. ISRM Symposium, Aachen, pp. 71–83.

Menzel, W. and W. Schreiner. 1977. Zum geotechnischen Verhalten von Steinsalz verschiedener Lagerstätten der DDR, Teil II: Das Verformungsverhalten: Neue Bergbautechnik 7, pp. 565–571.

Odquist, F. K. G. and J. Hult. 1962. Kriechfestigkeit metallischer Werkstoffe: Springer Verlag. 303 pages.

Penny, R. K. and D. L. Mariott. 1971. Design for Creep: McGraw Hill, London. 291 pages.

Serata, S. and E. Gloyna. 1960. Principle of Structural Stability of Underground Salt Cavities. Journal of Geophysical Research (65), No. 9, pp. 2979–2987.